© 2018. Published by The Company of Biologists Ltd | Development (2018) 145, dev161042. doi:10.1242/dev.161042

STEM CELLS AND REGENERATION

RESEARCH ARTICLE

GSK-3 promotes S-phase entry and progression in *C. elegans* germline stem cells to maintain tissue output

Tokiko Furuta[1,*], Hyoe-Jin Joo[1,*], Kenneth A. Trimmer[1,2,*], Shin-Yu Chen[1] and Swathi Arur[1,2,†]

ABSTRACT

Adult *C. elegans* germline stem cells (GSCs) and mouse embryonic stem cells (mESCs) exhibit a non-canonical cell cycle structure with an abbreviated G1 phase and phase-independent expression of Cdk2 and cyclin E. Mechanisms that promote the abbreviated cell cycle remain unknown, as do the consequences of not maintaining an abbreviated cell cycle in these tissues. In GSCs, we discovered that loss of *gsk-3* results in reduced GSC proliferation without changes in differentiation or responsiveness to GLP-1/Notch signaling. We find that DPL-1 transcriptional activity inhibits CDK-2 mRNA accumulation in GSCs, which leads to slower S-phase entry and progression. Inhibition of *dpl-1* or transgenic expression of CDK-2 via a heterologous germline promoter rescues the S-phase entry and progression defects of the *gsk-3* mutants, demonstrating that transcriptional regulation rather than post-translational control of CDK-2 establishes the abbreviated cell cycle structure in GSCs. This highlights an inhibitory cascade wherein GSK-3 inhibits DPL-1 and DPL-1 inhibits *cdk-2* transcription. Constitutive GSK-3 activity through this cascade maintains an abbreviated cell cycle structure to permit the efficient proliferation of GSCs necessary for continuous tissue output.

KEY WORDS: GSK3β, Cell cycle, Germ cells, Stem cell proliferation

INTRODUCTION

Stem cells sustain tissue development and growth, and maintain tissue homeostasis by balancing the rates of proliferation and differentiation (Morrison and Spradling, 2008). *Caenorhabditis elegans* adult germline stem and progenitor cells (stem cells and their proliferative progeny, henceforth referred to collectively as GSCs) support gamete production and sustain germline development by maintaining this balance (Hansen and Schedl, 2013). GSCs exhibit two intrinsic properties that help sustain the growth of the germline: they undergo constant self-renewal in a Notch signaling pathway-dependent manner (Austin and Kimble, 1987; Berry et al., 1997); and they display a cell cycle structure with a very short G1 phase (henceforth referred to as an 'abbreviated' cell cycle) (Fox et al., 2011). Mechanisms that promote the abbreviated cell cycle remain unknown, as do the consequences of not maintaining an abbreviated cell cycle in this tissue.

[1]Department of Genetics, University of Texas MD Anderson Cancer Center, Houston, TX 77030, USA. [2]Genes and Development Graduate Program, MD Anderson Cancer Center UT Health Graduate School of Biomedical Sciences, Houston, TX 77030, USA.
*These authors contributed equally to this work

[†]Author for correspondence (sarur@mdanderson.org)

S.A., 0000-0002-6941-2711

Received 26 October 2017; Accepted 17 April 2018

Although GSCs represent an adult stem cell population, they are more similar to mouse embryonic stem cells (mESCs) with respect to cell cycle structure and regulation (Fox et al., 2011; White and Dalton, 2005). This supports the idea that the cell cycle characteristics of stem cells reflect the demands of the tissues they support rather than the stage of the organism from which the cells are derived. For example, the adult mammalian satellite cells (muscle stem cells) and bulge stem cells (hair follicle stem cells) are required for tissue regeneration and thus remain quiescent (G0) for most of their adult life. However, when their host tissue is stressed or damaged, they re-enter the cell cycle and undergo G1, S, G2 and M phases to repopulate the tissue, after which they re-enter quiescence, effectively meeting the demands of the tissue (Cotsarelis et al., 1990; Schultz, 1974, 1985; Snow, 1977). In contrast, early embryonic cells from *C. elegans*, *D. melanogaster* and *X. laevis* require rapid expansion, and thus abbreviate both gap (G1 and G2) phases, which, when coupled with rapid DNA replication, results in an exceedingly fast cell cycle that is necessary to generate the requisite number of cells for the onset of early gastrulation events (Edgar and McGhee, 1988; Graham, 1966a,b; Kermi et al., 2017; Takada and Cha, 2011). Although mESCs also display rapid expansion in culture, they maintain a G2 phase and S-phase length similar to that of differentiated mouse somatic cells (Stead et al., 2002). Instead, their rapid expansion is due to an abbreviated G1 phase, allowing these cells to cycle rapidly while protecting their DNA through the intra-S and G2 checkpoints (Chuykin et al., 2008; Stead et al., 2002; White and Dalton, 2005). Likewise, GSCs abbreviate the G1 phase (Fox et al., 2011) while retaining the G2 checkpoints (Garcia-Muse and Boulton, 2005; Seidel and Kimble, 2015). As the *C. elegans* germline continuously produces oocytes while sperm is available (Jaramillo-Lambert et al., 2007), the GSCs likely meet the constant demand for gametes by shortening their G1 phase and abbreviating their cell cycle to increase the rate of proliferation. This abbreviated cell cycle is seemingly regulated differently from the canonical somatic cell cycle.

Unlike somatic cells, in which the G1 phase is marked by oscillating cyclin expression (Aleem et al., 2005; Guevara et al., 1999), G1 phase in the abbreviated cell cycle structure of both GSCs and mESCs is seemingly absent, with stem cells displaying a phase-independent expression of the G1/S regulators CDK2 and cyclin E (Fox et al., 2011; White and Dalton, 2005). However, a mechanism for sustaining an abbreviated cell cycle structure with an abbreviated G1 remains unresolved. Here, we describe the consequences of abnormal S-phase entry and progression, and the mechanism through which constitutive GSK-3 activity (glycogen synthase kinase 3 beta or GSK3β in mammals) promotes G1/S progression in GSCs to maintain constant growth in the tissue.

GSK3β functions in several signaling pathways, such as the insulin, TOR and Wnt pathways, to regulate proliferation, differentiation and apoptosis (Bouskila et al., 2008; Campbell et al., 2012; McManus et al., 2005; Parisi et al., 2011), in addition to

Development (2018) 145, dev161042. doi:10.1242/dev.161042

its original role of inhibiting glycogen synthase (Larner et al., 1968; Rylatt et al., 1980). Although GSK3β is known to promote differentiation of mESCs via the inhibition of pluripotency factors through β-catenin (Ying et al., 2008), we describe here for the first time its role in promoting a unique cell cycle structure shared by *C. elegans* GSCs, mESCs and possibly other tissues. We discovered that GSCs maintain an abbreviated G1 owing to continuously high Cdk2 (*C. elegans* CDK-2) mRNA expression, such that in wild-type worms GSK-3 is constitutively active, CDK-2 is constantly high and GSCs are continuously poised to enter and progress through S phase. We show that GSK-3 inhibits DPL-1 transcription factor, which in turn inhibits *cdk-2* mRNA accumulation; thus, under constitutively high activity of GSK-3, DPL-1 is inhibited and CDK-2 levels are persistently high, revealing a mechanism that drives the unique cell cycle structure of GSCs. Loss of *gsk-3* results in a reduction of CDK-2 in GSCs, leading to slower entry and progression of S phase, and reducing tissue output. Thus, GSK-3 promotes an abbreviated cell cycle structure to permit the continuous proliferation of GSCs for gamete production.

RESULTS

GSK-3 promotes GSC proliferation in a germline-autonomous and kinase-dependent manner during larval and adult development

The adult wild-type *C. elegans* germline harbors a population of ∼200-250 GSCs (stem cells and their proliferative progeny, henceforth referred to collectively as GSCs) that are maintained by Notch signaling (Berry et al., 1997; Crittenden et al., 2003; Fox and Schedl, 2015; Fox et al., 2011; Kimble and Crittenden, 2005) and can be assayed by labeling with REC-8 [a stem cell-specific marker (Hansen et al., 2004)] or by absence of HIM-3 [a meiotic-specific marker (Zetka et al., 1999)] (Fig. 1A-B, Fig. S1). As the GSCs move away from the distal tip cell (DTC) (Fig. 1A, Fig. S1), they differentiate and enter meiosis, at ∼20-22 cell diameters, in both L4 and adult germlines. Characterization of two strong loss-of-function alleles of *gsk-3* (*nr2047* and *tm2223*) (see supplementary Materials and Methods) revealed that adult *gsk-3* mutant germlines contained ∼90 GSCs, compared with the ∼200-250 found in wild-type (Fig. 1B,C, Fig. S1). However, the GSCs entered meiosis ∼20-22 cell rows away from the DTC in the *gsk-3* mutants, similar to wild type (Fig. 1B,D, Fig. S1). To determine whether the defect in GSC accumulation in *gsk-3* mutant animals occurred throughout development, or whether it occurred only in adults, we analyzed earlier developmental time-points. We found that the number of germ cells in the two *gsk-3* mutant alleles was significantly reduced as early as L3, with ∼14 germ cells compared with the wild-type ∼34 germ cells (Table S1). At the L4 stage and into adulthood, the GSCs in *gsk-3* mutants remained at ∼90 (Fig. 1C). This failure to expand the progenitor population suggested that the germline output would also be reduced. To determine whether the lower number of GSCs in the *gsk-3* mutant resulted in a decrease of tissue output, we assayed the number of oocytes produced in the mutant by counting the number of oocytes marked by RME-2 labeling, a yolk receptor. We found that *gsk-3* mutants contain fewer developing oocytes throughout adulthood when compared with wild type (Fig. 1E,F). Taken together, the GSCs fail to expand in number in the *gsk-3* mutants from early larval stages on into adulthood, possibly leading to a decrease in germ cell output.

To test whether the GSC defect was due to a germline-autonomous function of *gsk-3*, we generated two germline-specific GFP::GSK-3 transgenes, driven by either the *pie-1* or the *mex-5* promoter, referred to here as GFP::GSK-3 (WT) (Fig. S2A,B). Expression of either germline specific GFP::GSK-3 (WT) transgene rescued the GSC defect in *gsk-3* mutants (Fig. 1G-I,), suggesting that the GSC defect is due to an autonomous function of GSK-3 in the germline.

To determine whether GSK-3 kinase activity was necessary for GSC proliferation, we generated a kinase-dead transgene by mutating the kinase core residues (K65, E77, D161 and D180) to alanine (Doble and Woodgett, 2003) (see supplementary Materials and Methods). The resulting transgene, GFP::GSK-3 (K65A, E77A, D161A and D180A), referred to here as GFP::GSK-3 (KD), is driven by the *mex-5* germline-specific promoter and is inserted at the identical chromosomal location to GFP::GSK-3 (WT) using the MosSci integration system on Chromosome II (see supplementary Materials and Methods). Whereas GFP::GSK-3 (WT) and GFP::GSK-3 (KD) are expressed at the same level and in similar cellular compartments in the progenitor zone (Fig. S2C), we find that, unlike the wild-type transgene, GFP::GSK-3 (KD) did not rescue the GSC defects (Fig. 1H-J). These data together demonstrate that *gsk-3* functions germline-autonomously in a kinase-dependent manner to promote GSC proliferation in the germline.

We next addressed the issue of whether the defects in GSCs occur as a consequence of increased differentiation, loss of self-renewal or a cell cycle defect. The GSC defect is likely not due to increased differentiation, as meiotic entry was maintained at 20-22 cell diameters from the DTC in both wild-type and *gsk-3* mutants (Fig. 1D,I and Fig. S1). Therefore, we next investigated whether the *gsk-3* mutant GSCs remained responsive to Notch signaling for self-renewal.

gsk-3 mutant GSCs remain responsive to Notch signaling

To determine whether the *gsk-3* mutant GSCs respond to Notch signaling, we assayed *gsk-3* mutant GSCs in conditions with decreased or increased Notch receptor (GLP-1) activity by using the *glp-1* temperature-sensitive alleles *bn18ts* (reduction of function) and *ar202gf* (gain of function). To determine the effect of loss of *glp-1* signaling on *gsk-3* mutant GSCs we used *glp-1(bn18ts)* with *gsk-3(nr2047)*. At the permissive temperature of 15°C, *glp-1(bn18ts)* and *gsk-3(nr2047);glp-1(bn18ts)* germlines produce GSCs as well as meiotic cells, as assayed by labeling with HIM-3 to mark the meiotic cells (Fig. 2A,C,E,G). However, shifting *glp-1(bn18ts)* or *gsk-3(nr2047);glp-1(bn18ts)* mutants as embryos to the restrictive temperature of 25°C results in loss of the GSC population with only sperm being produced in 100% of adult germlines (Fig. 2F,H). Wild type or *gsk-3(nr2047)* mutants at 25°C are indistinguishable from their 15°C counterparts. These data suggest that the *gsk*-3 mutant GSCs require *glp-1* activity to self-renew.

To determine the impact of increased *glp-1* Notch signaling on *gsk-3* mutant GSCs, we assayed *glp-1(ar202gf)* with *gsk-3(nr2047)*. Adult *glp-1(ar202gf)* mutant and *gsk-3(nr2047);glp-1(ar202gf)* mutant germlines at the permissive temperature of 15°C have GSCs and meiotic cells (Fig. 2I,K). In contrast, shifting *glp-1(ar202gf)* or *gsk-3(nr2047);glp-1(ar202gf)* mutants as embryos to the restrictive temperature of 25°C results in adult tumorous germlines (Fig. 2J,L). Although, the *gsk-3(nr2047);glp-1(ar202gf)* mutant tumors appear 'skinnier' (with respect to the size of the gonads) relative to *glp-1(ar202gf)* single mutant tumors (Fig. 2J,L). These data indicate that *glp-1* activity is sufficient to drive self-renewal at the expense of differentiation in *gsk-3* mutants. Together, these data demonstrate that *gsk-3* mutant GSCs remain responsive to *glp-1* signaling. As neither differentiation nor self-renewal was affected in *gsk-3* mutant GSCs, we investigated their cell cycle parameters.

Development (2018) 145, dev161042. doi:10.1242/dev.161042

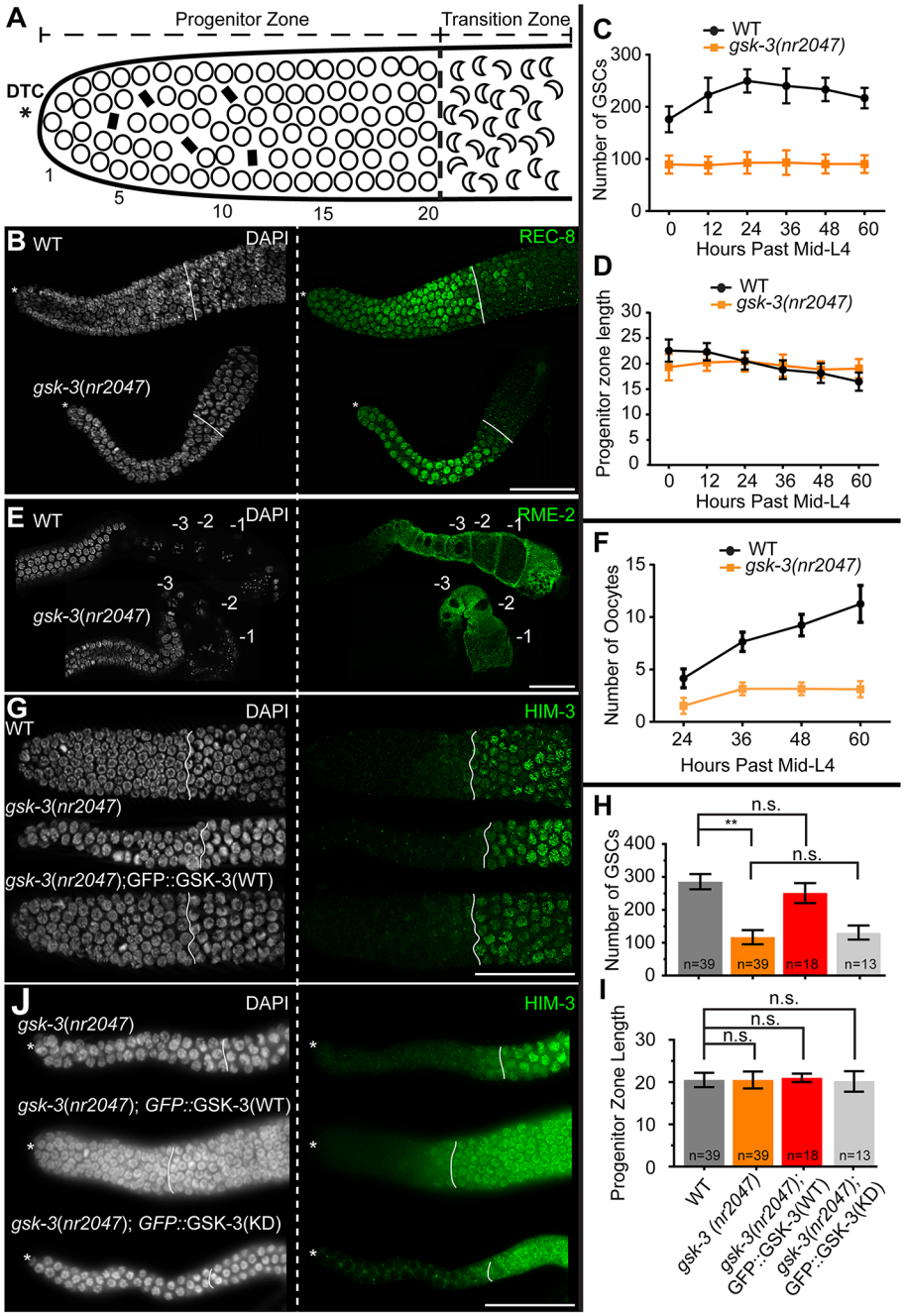

Fig. 1. GSK-3 regulates the accumulation of germline stem cells. (A) Schematic representation of the progenitor zone of an adult hermaphroditic germline. The asterisk marks the DTC (distal tip cell). Each circle and black bar is a GSC. The progenitor zone, which is 20-22 cell diameters, harbors a population of 200-250 GSCs. Black bars represent GSCs undergoing mitosis. GSCs enter meiosis (crescent moon) and differentiate 20-22 cell diameters away from the DTC. (B) Dissected germlines from adult (24 h past L4) wild-type (top) and *gsk-3(nr2047)* (bottom) labeled with REC-8 (green, GSCs) and DAPI (white, DNA). (C) Quantitation of the total number of GSCs (positive REC-8 staining) in *gsk-3(nr2047)* and wild-type germlines from mid-L4 until 60 h after mid-L4. (D) Quantitation of the progenitor zone length from wild-type and *gsk-3(nr2047)* at mid-L4 and adult stages of development. (E) Proximal region of dissected germlines with the end of the pachytene on the left and the −1 oocyte on the right, labeled with RME-2 (green, oocytes) and DAPI (white, DNA). (F) Time course analysis of the number of RME-2-positive cells (oocytes) in the germline from 24 h after L4 to 60 h after L4. (G) Transgenic expression of a wild-type GFP::GSK-3 driven via the *pie-1* promoter (*vizIs27[Ppie-1::GFP::GSK-3(WT)]*) rescues GSC defects of *gsk-3* mutant animals. (H) Quantitation of GSCs from *gsk-3* mutant animals with and without the wild-type and kinase-dead GFP::GSK-3 transgenes. (I) Quantitation of the progenitor zone length from *gsk-3* mutant animals with and without the wild-type and kinase-dead GFP::GSK-3 transgenes. (J) Transgenic single copy GFP::GSK-3 (*vizSi44[Pmex-5::GFP::GSK-3* [WT]) rescues *gsk-3* mutant GSC defects, whereas GFP::GSK-3 (KD) (*vizSi20[Pmex-5::GFP::GSK-3]* [K65A,E77A,D180A,D161A]) does not. The somatic phenotypes (Gleason et al., 2006; Maduro et al., 2001) of *gsk-3* mutants are not rescued with either transgene, likely due to lack of promoter activity in these tissues (not shown). *x*-axes are identical for H and I, and are shown in I. Each experiment was performed at least three times. For C, D and F, 30 germlines were assayed each time. Error bars indicate s.d. The end of each progenitor zone is labeled with a solid line. $^{**}P<0.0001$; n.s., not significant. Scale bars: 40 µm.

gsk-3 mutant GSCs enter and progress through S phase inefficiently

To determine the cell cycle parameters of the *gsk-3* mutant GSCs, we analyzed the cell cycle phases via immunofluorescence analysis of phospho-histone H3 (pH3) labeling to mark M phase and EdU incorporation to mark S phase (see Materials and Methods). GSCs from both *gsk-3* mutant and wild-type adult and mid-L4 germlines contained pH3-positive cells (Fig 3A-C). The number of pH3-positive nuclei in wild-type gonads ranged from 4-13 and *gsk-3* mutant gonads ranged from 0-9, with no statistically significant difference in the average mitotic index of *gsk-3* mutant GSCs compared with wild type (Fig. 3C, Fig. S1). These data indicate that GSCs in *gsk-3* mutants enter productive M phase. In contrast, S phase appeared markedly altered in *gsk-3* mutants. Whereas 100% of wild-type germlines incorporate EdU and display an S-phase index of ~55% upon 30 min of feeding the EdU bacteria (Fig. 3A, Fig. S3), over 90% of the *gsk-3* mutant germlines failed to incorporate detectable EdU as either adults (Fig. 3A) or mid-L4s (Fig. 3B). Of those germlines that did incorporate EdU, the levels of EdU were very low per germ cell, based on the label intensity. The S-phase index of those germlines with low EdU-incorporating cells was ~6% (Fig. 3D). The rate of detectable EdU incorporation did not change in the *gsk-3* mutant even upon longer EdU feeding of 1 h, 3 h or 5 h (Fig. S3). Because the standard method in the field uses feeding of EdU bacteria as a tool for EdU incorporation, it is possible that the feeding rate of *gsk-3* mutants affected this analysis. To investigate this possibility, we used *eat-2* mutants, which have a lower feeding rate, together with *gsk-3* mutants to assay whether feeding rate affects EdU incorporation. Whereas *eat-2* mutants have a reduced pharyngeal pumping rate of only ~77 pumps/min compared with a wild-type rate

Development (2018) 145, dev161042. doi:10.1242/dev.161042

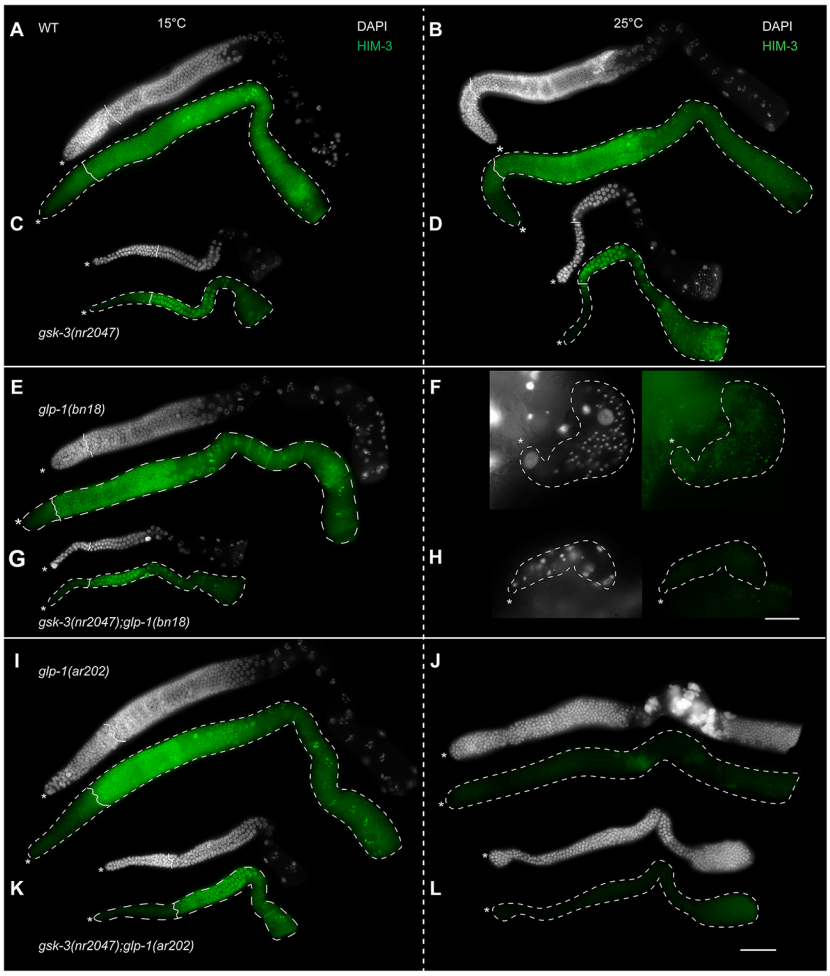

Fig. 2. *gsk-3* mutant GSCs respond to GLP-1/Notch signaling. Composite images of dissected germlines from adult (24 h after L4) animals of indicated genotypes labeled with DAPI (white, DNA) and HIM-3 (green, meiotic cells) oriented from left (progenitor zone) to right (oocytes). (A,C,E,G,I,K) Micrographs of germlines from animals maintained at the permissive temperature of 15°C; (B,D,F,H,J,L) Adult germlines from animals shifted to the restrictive temperature of 25°C as embryos. (A,B) Wild-type germlines contain GSCs and meiotic cells both at 15°C and 25°C. (C,D) *gsk-3(nr2047)* mutant germlines contain GSCs and meiotic cells at 15°C and 25°C. The *gsk-3* mutant germlines are smaller compared with wild type. (E,F) *glp-1(bn18ts)* mutant germlines harbor GSCs and meiotic cells at 15°C, but have only sperm at 25°C. (G,H) *gsk-3(nr2047);glp-1(bn18ts)* double mutant germlines harbor both GSCs and meiotic cells at 15°C but only sperm at 25°C. (I,J) *glp-1(ar202gf)* mutant germlines harbor both GSCs and meiotic cells at 15°C, but generate adult tumorous germlines at 25°C. (K,L) *gsk-3(nr2047);glp-1(ar202gf)* double mutants have GSCs and meiotic cells at 15°C, and generate tumors at 25°C. Each experiment was performed three times and 30 germlines were assayed each time. Germlines are outlined with a dashed line. The end of each progenitor zone is labeled with a solid line. Scale bars: 20 µm in F,H; 50 µm in A-E,G,I-L.

of ~274 pumps per minute, *gsk-3* mutants displayed a rate of ~204 pumps/min (Fig. S4). However, despite a 72% reduction in pharyngeal pumping rate in *eat-2* mutant animals, 100% of the *eat-2* mutant germlines incorporated the robust EdU label on 'feeding' (Fig. S4), suggesting that feeding rate is not affecting EdU incorporation in the *gsk-3* mutant. In addition, we developed an assay that did not involve feeding, and instead soaked the wild-type and mutant *gsk-3* animals in an EdU solution for 10 min (see Materials and Methods). As with feeding of EdU, 100% of wild-type animals displayed robust EdU incorporation with an S-phase index of ~60%, whereas *gsk-3* mutant germlines continued to display low/no EdU incorporation. We use the soaking method of EdU detection for the remainder of this paper (Figs 4-6, Fig. S8).

The failure of a majority of *gsk-3* mutant germlines to incorporate detectable EdU suggests that GSCs in *gsk-3* mutants incorporate fewer molecules of EdU per GSC compared with wild-type GSCs, possibly because they are either entering or progressing through S phase more slowly. Additionally, some of the GSCs in the *gsk-3* mutant germlines displayed variable cell size, a few of which are reminiscent of GSC arrest (Fig. S5). These data suggest that the cell cycle defects in *gsk-3* mutant animals are a combination of slow entry and progression through the S phase, with some GSCs that may be arrested in G1. However, because the *gsk-3* mutant germline continued to produce sperm (during L4, Fig. 2), oocytes (during adulthood, Fig. 2) and embryos (Shirayama et al., 2006), we hypothesize that at least some of the *gsk-3* mutant GSCs continue to progress through the cell cycle.

To determine whether the GSCs in *gsk-3* mutant animals were arrested or delayed in G1, leading to inefficient S-phase entry, we assayed for subcellular GFP::MCM-3 (*gtIs64*) localization (Sonneville et al., 2012). MCM3 is a component of the pre-replication complex that accumulates in the nucleus in early-mid G1 in vertebrate cultured cells, and is phosphorylated by CDK2 and re-localized to the cytoplasm in late G1 or early S to prevent re-replication (Li et al., 2011); thus, nuclear localization of MCM3 indicates nuclei in G1 (Blow, 1993; Chong and Blow, 1996). To test whether GFP::MCM-3 had cellular localization dynamics in *C. elegans* GSCs similar to vertebrate cultured cells, we depleted *cdk-2* in GFP::MCM-3 animals and determined its localization. As previously described (Fox et al., 2011), depletion of *cdk-2* caused G1 cell cycle arrest wherein all cells were negative for EdU (S phase) and pH3 (M phase) (Fig. S6). GFP::MCM-3 localized to the GSC nuclei upon depletion of *cdk-2* (Fig. 3F,F′), indicating that GFP::MCM-3 changed cellular localization in GSCs in response to loss of *cdk-2*, and by extension G1 arrest, as would be predicted from the vertebrate system. Additionally, GFP::MCM-3 was excluded from meiotic germ cell nuclei in animals treated with *cdk-2* RNAi (Fig. 3F,F″, Fig. S6), indicating that the reporter changed localization based on the phase of the mitotic cell cycle. Consistent with previous reports that the GSCs display a very short (seemingly absent) G1 phase, wild-type germlines exhibit cytoplasmic GFP::MCM-3 in both GSCs and meiotic cells (Fig. 3E-E″). In contrast, GFP::MCM-3 was nuclear in *gsk-3* mutant GSCs (Fig. 3G,G′) in 56±3% of the cells (calculated from

Development (2018) 145, dev161042. doi:10.1242/dev.161042

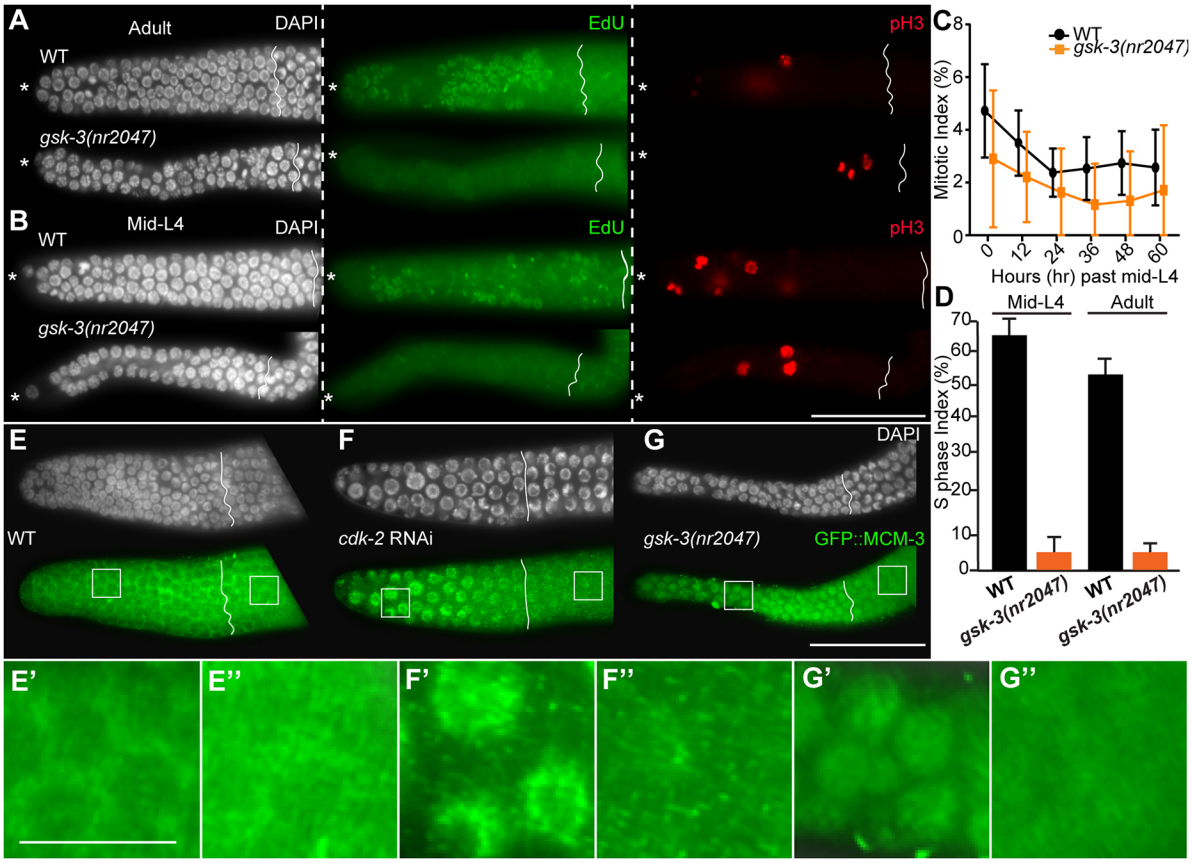

Fig. 3. *gsk-3* regulates entry into and progression through S phase in GSCs. Dissected germlines displaying the DTC on the left (asterisks). (A,B) *gsk-3* mutant and wild-type GSCs from adult (24 h after L4) and mid-L4 germlines labeled for M phase (pH3, red) and S phase (EdU, green). Germlines for mutants and wild type were processed in the same tube, and pictures taken at constant exposure and gain to compare the level of EdU incorporation. (C) Quantitation of the mitotic index from wild-type and *gsk-3* mutant germlines. The number of M-phase nuclei in wild-type gonads ranged from 4 to 13 and in *gsk-3* mutant gonads ranged from 0 to 9. The M-phase index between the wild-type and *gsk-3* mutant gonads is not significantly different. Forty germlines were analyzed for each time point. (D) *gsk-3* mutant GSCs with very low but detectable EdU incorporation exhibit an S-phase index of ~6% versus ~55% strong EdU incorporation in wild-type (adult) and ~67% (mid-L4) germlines. (E-G″) GFP::MCM-3(*gtIs64*) (green) localizes to the cytoplasm in wild-type GSCs. GFP::MCM-3 is localized to the nucleus in *cdk-2* RNAi and *gsk-3* mutant GSCs, but is cytoplasmic in the meiotic cells from these genotypes. The boxed areas in E-G are shown at higher magnification in E′-G″. Each experiment in A-D was performed five times; at least 30 germlines were assayed each time. Experiments in E-G″ were performed three times and 25 germlines were assayed each time. Error bars represent s.d. The end of each progenitor zone is labeled with a solid line. Scale bars: 40 µm.

over 20 germlines), and was cytoplasmic when the cells entered meiosis (Fig. 3G,G″). Taken together, these data suggest that *gsk-3* mutant GSCs are either arrested in G1 phase of the cell cycle or linger in G1 for a longer period relative to wild type due to inefficient entry into S phase. Additionally, increased nuclear GFP::MCM-3 suggests that CDK-2 activity may be affected in *gsk-3* mutants, which could result in the observed proliferation defects.

GSK-3 promotes *cdk-2* transcription to regulate rapid S-phase entry and progression

CDK-2 and cyclin E (CYE-1) are expressed and active in all wild-type GSCs (Fox et al., 2011). Thus, to determine whether CDK-2 function was reduced in *gsk-3* mutant germlines, we tested the expression of CYE-1 and CDK-2. We found that the protein expression pattern of CYE-1 in *gsk-3* mutant germlines was similar to wild type even though the levels appeared slightly lower in *gsk-3* mutant germlines (not significant) (Fig. S7). As no CDK-2 antibody exists, we obtained a transgenic YFP::CDK-2 (Cowan and Hyman, 2006) driven by the germline-specific *pie-1* promoter and expressed it in the *gsk-3* mutant background to assess its localization. Surprisingly, the transgenic expression of YFP::CDK-2 rescued GSC numbers (Fig. 4A-E) and S phase onset and progression in both L4 (Fig. S8) and adult germlines in *gsk-3* mutants (Fig. 4A-D,F). Additionally, CDK-2 is expressed throughout the GSCs in both wild-type and *gsk-3* mutant cells in this context (Fig. 4G,H). Because *pie-1*-driven YFP::CDK-2 rescued the *gsk-3* mutant GSC defects and localized to the *gsk-3* mutant GSCs in a manner similar to wild type, it suggested that the defects in *gsk-3* mutants are driven by abnormal CDK-2 function and that the relevant regulation of CDK-2 via GSK-3 was not through post-translational mechanisms, such as regulating CDK-2 protein degradation or activity through phosphorylation. Together, these data demonstrate that *gsk-3* mutant GSCs enter and progress through S phase abnormally due to lower CDK-2 accumulation, likely at the transcriptional level.

To determine whether GSK-3 regulates CDK-2 levels transcriptionally in the GSCs, we assayed CDK-2 mRNA in dissected germlines from *gsk-3* and wild-type animals, using qRT-PCR (see Materials and Methods). CDK-2 mRNA levels were tenfold lower in *gsk-3* mutant germlines compared with wild type (Fig. 4I) and were restored in *gsk-3* mutant animals carrying the transgenic YFP::CDK-2 (Fig. 4I). To determine whether the lower transcript level of CDK-2 in *gsk-3* mutant germlines was specific to the

Development (2018) 145, dev161042. doi:10.1242/dev.161042

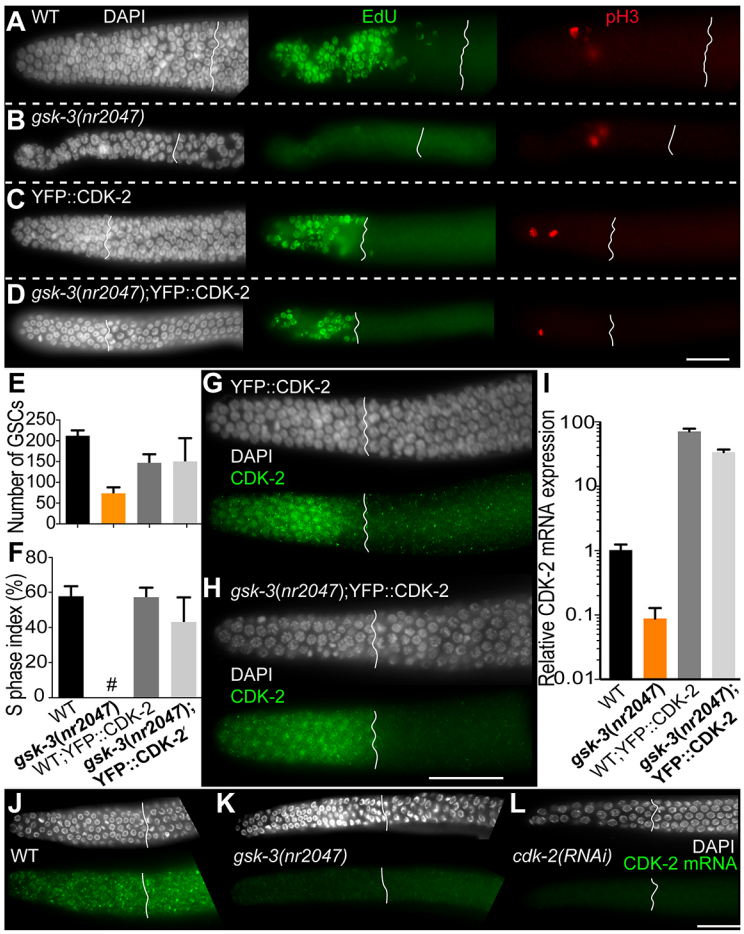

Fig. 4. CDK-2 transgenic expression via a germline promoter rescues the *gsk-3* germline stem cell proliferation defect. Dissected germlines displaying the DTC on the left (asterisks). (A-D) EdU incorporation (green), via the soaking method, in germlines from wild-type or *gsk-3* mutant animals with transgenic YFP::CDK-2 (*ddIs30*, via Ppie-1 promoter). (E) Quantitation of the total number of GSCs in germlines from wild-type and *gsk-3* mutants with transgenic YFP::CDK-2 expression. (F) Quantitation of the S-phase index from wild-type and *gsk-3* mutant GSCs with transgenic YFP::CDK-2 expression. *x*-axis labels are the same for both graphs. # indicates that the EdU signal was below the detection limit for a majority of the germlines. (G,H) Expression of YFP::CDK-2 in the GSCs of wild-type and *gsk*-3 mutant animals visualized with anti-GFP antibody staining. (I) qRT-PCR of *cdk-2* mRNA on *gsk-3* mutant germlines with or without the YFP::CDK-2 transgene relative to wild type. YFP::CDK-2 transgene in wild-type background has higher *cdk-2* mRNA compared with wild type, revealing overexpression of CDK-2 in the transgene. (J-L) *cdk-2* fluorescence *in situ* hybridization analysis on dissected germlines from wild-type (J), *cdk-2* depleted (L) and *gsk-3* mutant (K) germlines. In A-H, the experiments were performed four times and each time 30-35 germlines were analyzed. In I, the experiment was performed three times and each time 100 germlines were dissected and assayed by qRT-PCR. (J-L) The experiment was performed three times and each time 12-15 germlines were assayed. Error bars indicate s.d. All experiments were performed on adult animals 24 h after the L4 stage of development. The end of each progenitor zone is labeled with a solid line. Scale bars: 40 µm.

progenitor zone, we performed single-molecule hairpin chain reaction FISH (Shah et al., 2016) using CDK-2 mRNA probes in wild-type and *gsk-3* mutant germlines. CDK-2 mRNA accumulates throughout the progenitor zone, predominantly in the cytoplasm, and is specific to *cdk-2* (Fig. 4J,L). However, in *gsk-3* mutant germlines, *cdk-2* mRNA levels are much lower relative to wild-type germlines (Fig. 4K). These data demonstrate that GSK-3 promotes *cdk-2* mRNA levels in the wild-type progenitor zone.

To directly assess whether GSK-3 regulates the transcription of CDK-2, we designed a transcriptional reporter for CDK-2. Perusal of the CDK-2 gene structure on Wormbase (www.wormbase.org, ver WS258), however, revealed that intron 1 (Fig. 5A), rather than the promoter annotated by Wormbase, contained multiple transcription factor- and RNA polymerase II-binding sites, as well as an SL1 splice site (Wormbase WS258) (Fig. S9A). These observations suggested that intron 1, rather than the promoter, may drive CDK-2 expression. Thus, we generated two distinct transgenes: one with the Wormbase predicted 2 kb promoter driving GFP (*cdk-2[Pr::GFP]*), and one containing the intron 1 driving GFP (*cdk-2[In1]::GFP*) (Fig. 5A). As hypothesized, we observed that *cdk-2[Pr]::GFP* did not express in the germline, suggesting that the predicted promoter does not drive *cdk-2* expression (*vizSi34*, data not shown, Wormbase WS258). Instead, *cdk-2[In1]::GFP* was expressed throughout the germline (Fig. 5B), suggesting that intron 1 drives *cdk-2* expression in the germline. In comparison with wild type, expression of *cdk-2[In1]::GFP* in *gsk-3* mutants resulted in lower GFP accumulation of the reporter in the distal region, but not in oocytes (Fig. 5C,D). These data demonstrate that GSK-3 regulates CDK-2 transcription in the GSCs.

DPL-1 represses CDK-2 expression and S-phase entry and progression in GSCs, and is inhibited by GSK-3

To determine the factors that regulate CDK-2 transcription downstream of GSK-3, we perused the chromatin immunoprecipitation (ChIP) data for the CDK-2 intron 1 using Wormbase and ModEncode (Elsner and Mak, 2011; Muers, 2011). This analysis identified several transcription factors that bind to intron 1 of CDK-2, most notably LIN-35, EFL-1 and DPL-1 (Fig. S9A), all of which promote S-phase entry in vertebrate systems (Almasan et al., 1995; Muller et al., 1997). Because loss of *lin-35*, *efl-1* or *dpl-1* individually does not inhibit S phase in *C. elegans* (Ceol and Horvitz, 2001; Chi and Reinke, 2006, 2009), it suggested to us that they do not promote S phase in *C. elegans*. Thus, we wondered whether each of these transcription factors represses rather than promotes S phase in the context of GSK-3. To determine whether these factors regulate *cdk-2* mRNA and thus S-phase entry and progression downstream to *gsk-3*, we assayed them via RNAi-mediated depletion in the *gsk-3* background. Depletion of *dpl-1* in L4 animals from wild-type or *gsk-3* heterozygous animals resulted in strong embryonic lethality in F1 progeny, as did the double mutants between *dpl-1* and *gsk-3* (not shown). Thus, we depleted *dpl-1* starting at L4 in wild-type and *gsk-3* mutant animals for 48 h and assayed for EdU incorporation in the germlines using the EdU soaking method (Fig. S9B). Wild-type germlines from control (luciferase) RNAi and *dpl-1* RNAi exhibited normal EdU incorporation with S-phase indices of ∼55% and ∼67%, respectively (Fig. 6A,C, Fig. S9C), as well as endomitotic oocytes in the proximal germlines, as described previously (Chi and Reinke, 2009). *dpl-1* RNAi in *gsk-3* mutant animals restored EdU

Development (2018) 145, dev161042. doi:10.1242/dev.161042

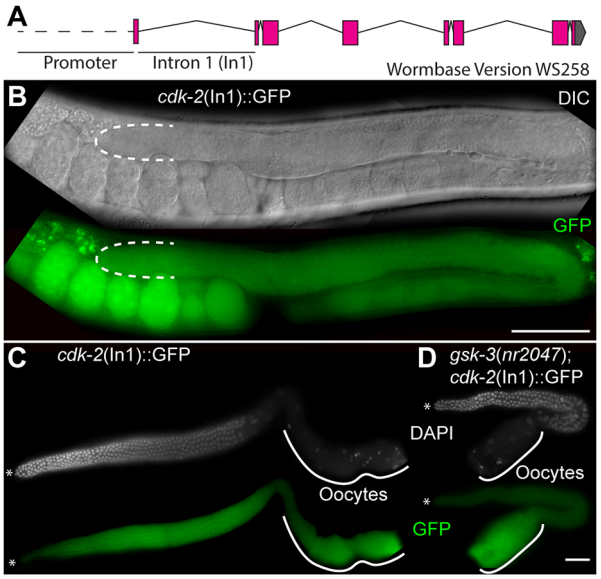

Fig. 5. CDK-2 is transcriptionally regulated in a *gsk-3*-dependent manner in the germline. (A) Gene structure of *cdk-2* from Wormbase Ver WS258. The promoter and intron 1 are labelled. (B) Differential interference contrast (DIC) and GFP live imaging of the transcriptional reporter driven by intron 1 of *cdk-2* in the germline and embryos. Dashed line marks the outline of the distal germline. (C,D) Asterisk marks the DTC. Dissected germlines from adult (24 h after L4) wild type and *gsk-3* mutants harboring the *cdk-2* transcriptional reporter driven by the intron 1 reporter, mounted in PLP media (no GFP staining) on the same slide, with oocytes on the right (solid lines). Intron 1 of *cdk-2* drives GFP expression in the distal germline of wild type (C) but less so in the *gsk-3* mutant (D). Scale bars: 50 µm.

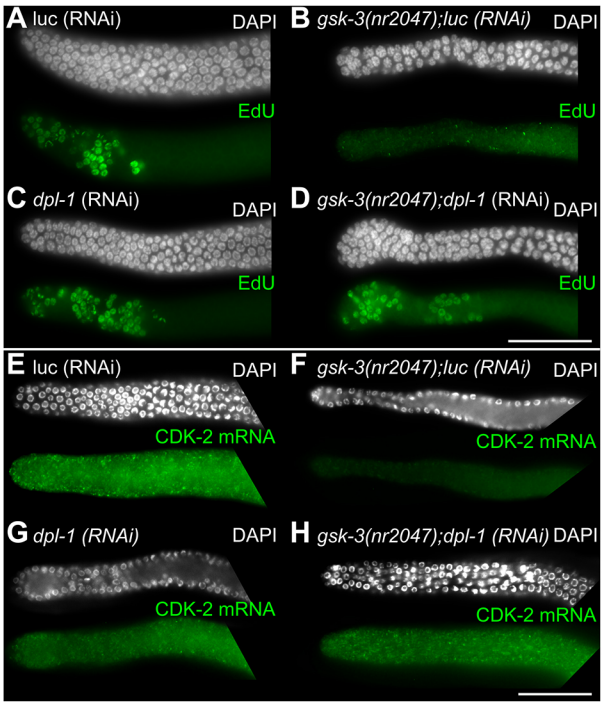

Fig. 6. GSK-3 inhibits DPL-1 to regulate *cdk-2* transcription and S-phase progression in *C. elegans* GSCs. Dissected adult (24 h after L4) germlines oriented with the DTC towards the left. (A-D) DNA is labeled in white (DAPI) and EdU (green) labels cells in S phase. EdU incorporation in germlines from *gsk-3* mutant animals with RNAi-mediated depletion of *dpl-1* (D) and luciferase (as control) (B). (E-H) DNA is labeled in white (DAPI) and *cdk-2* mRNA is labeled in green. *cdk-2* mRNA fluorescence *in situ* hybridization analysis from *gsk-3* mutant animals with RNAi-mediated depletion of *dpl-1* and luciferase (control). The photographs for *cdk-2* fluorescence *in situ* hybridization were captured with the same exposure time. The RNAi experiments were performed five times and 20-22 germlines in A-D and 10-12 germlines in E-H were imaged each time. Scale bars: 40 µm.

incorporation in all germlines with an S-phase index of ∼35% (Fig. 6B,D, Fig. S9C), partially rescuing the S-phase progression defect. These data suggest that *gsk-3* normally inhibits *dpl-1* in the GSCs to promote S-phase progression, likely through *cdk-2* transcriptional regulation.

To determine whether *dpl-1* regulated *cdk-2* mRNA levels, we performed FISH analysis on *gsk-3(nr2047);dpl-1(RNAi)* dissected germlines. We found that the *cdk-2* mRNA was restored in the *gsk-3(nr2047);dpl-1(RNAi)* double-mutant germlines and was equivalent to *dpl-1* RNAi alone (Fig. 6E-H). In summary, these data demonstrate that GSK-3 inhibits DPL-1 to maintain persistent high levels (and thus activity) of CDK-2 mRNA expression in wild-type GSCs, resulting in rapid S-phase entry and progression.

DISCUSSION

We report the mechanism through which *C. elegans* germline stem cells maintain their unique cell cycle structure with an abbreviated G1 phase. We show that consistent high and phase-independent expression of *cdk-2* mRNA is regulated by constitutive GSK-3 activity in the GSCs such that when the cells reach the end of mitotic M phase they can transition into S phase with minimal time spent in G1. Abbreviating the G1 phase of the cell cycle allows the cells to proliferate rapidly to meet the tissue demands imposed by continuous production of embryos. Our results also highlight that CDK-2 transcriptional control rather than post-translational control plays a central role in cell cycle phase transition from mitotic G1 to S in the *C. elegans* GSCs, thus uncovering a novel layer of cell cycle regulation.

We identified a role for GSK-3 in maintaining the abbreviated cell cycle structure via transcriptionally regulating *cdk-2* mRNA through inhibition of DPL-1. Loss of *gsk-3* function results in GSCs that progress through the cell cycle inefficiently, due to a longer time spent in G1, either because of slow progression or arrest in G1, coupled with slow replication and transition through the S phase. These defects result in a germline with fewer germ cells that is also shorter in length (Fig. 2), thus a 'skinny' germline, with fewer embryos produced. GSK-3 was originally described as a key metabolic regulator. However, in the context of the GSCs, our data suggests that GSK-3 is constitutively active and not regulated. In vertebrates, GSK3 is inactivated by phosphorylation at Serine 9 downstream to Insulin signaling (Sutherland et al., 1993). However, we find that in *C. elegans* GSK-3, the sequence around serine 9 is not conserved, suggesting that GSK-3 may be refractory to inactivation by Insulin signaling. In addition, we find that *gsk-3* mutant GSCs respond to nutritional deprivation similar to the wild-type mutant GSCs and arrest in G2 (Fig. S10; Seidel and Kimble, 2015). These observations suggest that the GSK-3 does not respond to the nutritional cues, and that the cell cycle arrest in *gsk-3* mutant GSCs is not at G2. In summary, our data suggests that GSK-3 may not be modified to regulate the cell cycle, but rather is constitutively high to ensure the rapid progression through G1 phase of the cell cycle, both under conditions of constitutive growth and when transitioning from poor environmental conditions to optimal ones. It is likely that the regulation of cell cycle in germline stem cells occurs predominantly at G2, such that the cell cycle structure is set up to maintain an abbreviated G1 under all conditions, and constitutive GSK-3 activity promotes CDK-2/cyclin E activity to facilitate this process (Fig. 7).

Development (2018) 145, dev161042. doi:10.1242/dev.161042

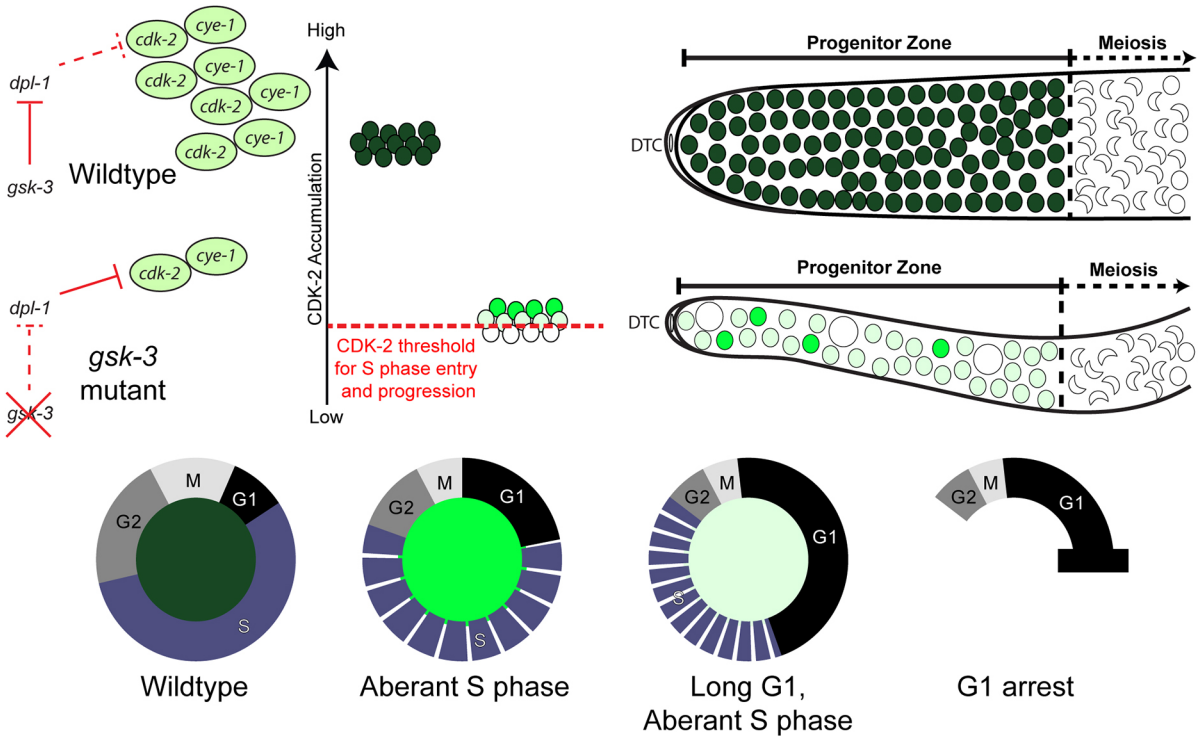

Fig. 7. Model. GSK-3 inhibits DPL-1 transcriptional repression to maintain persistent high levels of CDK-2 and promote a short G1 phase coupled with rapid S-phase entry and progression in *C. elegans* germline stem cells. (Left) Inhibitory cascade depicting the double-negative pathway, with *gsk-3* inhibiting *dpl-1*, which in turn inhibits *cdk-2* transcription. (Middle) CDK-2 accumulation axis, highest being at the top. Circles represent germ cells. Green intensity represents CDK-2 accumulation, with darker green being higher accumulation. (Right) Representative germline drawings for wild type and *gsk-3* mutants. Intensity of the green inside each nucleus represents the amount of CDK-2 accumulation in those nuclei. (Bottom) Cell cycle structures at different CDK-2 accumulation levels. In wild type (dark green), GSK-3 inhibits *dpl-1* so that CDK-2 is produced at levels far above the threshold for S-phase entry and progression in all cells. This allows all the germline stem cells to enter and progress efficiently (dark green circles). In *gsk-3* mutants, DPL-1 inhibits CDK-2 transcription, so that CDK-2 is reduced to or is below the threshold for S-phase entry and progression. Fluctuating levels of CDK-2 accumulation may lead to some nuclei (green and light green circles) progressing slowly, with an aberrant S phase or long G1 phase, while others (white circles) may arrest in G1, thus resulting in a germline with low tissue output.

How does constitutively high expression of CDK-2 regulate the G1/S switch?

We find that the *cdk-2* mRNA maintains a constitutively high level of expression in the GSCs, which is necessary for the abbreviated cell cycle structure. The expression of CDK-2 also reflects its activity, as shown previously by phospho-CDC-6 expression, and functional analysis (Fox et al., 2011) (this study). Using the nuclear to cytoplasmic shuttling of MCM-3 as a dynamic read out of CDK-2 function, we show that MCM-3 is nuclear when CDK-2 function is lower and cytoplasmic when CDK-2 function (or expression) is high. In *gsk-3* mutant GSCs, MCM-3 is nuclear in about 56% of the cells, the levels of *cdk-2* mRNA are significantly reduced and the cells incorporate EdU very inefficiently. Furthermore, overexpression of CDK-2 in the *gsk-3* mutants completely rescues the GSC defects. Together, these data suggest that in GSCs, the cell cycle at the G1/S boundary is largely regulated by the accumulation of CDK-2. Consistent with this is the observation that depletion (via RNAi) versus reduction of *cdk-2* mRNA result in two distinct phenotypes: cell cycle arrest in the former (Fox et al., 2011) and slow S-phase entry and progression in the latter (Fig. 7).

That CDK-2 expression levels regulate the G1/S switch may be unique to cells that have a short G1. To put this in the context of canonical mammalian cell cycle progression, which is regulated via low Cdk2 activity in G1 to enable pre-replication complexes to assemble at origins (Blow and Hodgson, 2002), we propose the following model. Canonically, inactive Cdk2 enables the loading of the pre-replication complex into the nucleus at the end of G1, and active Cdk2 then initiates S phase, both of which are regulated through post-translational mechanisms such as phosphorylation. In the context of GSCs, it is likely that different thresholds form distinct complexes of CDK-2 that mediate its differing roles in G1 and S. For example, it is likely that the pre-replication complex can form at a lower threshold of CDK-2 (mimicking an ‘inactive’ pool of Cdk2) but not at a threshold of CDK-2 that drives entry and progression through S phase (Fig. 7). Observations from mESCs support this model. In mESCs despite continuous high expression of Cdk2 and cyclin E, a subset of Cdk2 complexes are in fact ‘inactivated’ at G1, allowing pre-replication complexes to assemble transiently and permitting S-phase entry (Ohtsuka and Dalton, 2008). Additionally, these complexes are thought to be undetectable above the elevated Cdk2 expression (Ohtsuka and Dalton, 2008). Therefore, one possible hypothesis is that much as in mouse ES cells, different complexes of CDK-2 exist, and some of these are inactivated at late G1 (despite the high expression of CDK-2) in GSCs coupled with a very transient loading of the pre-replication complex. This notion of a very transient loading of the licensing complex may account for the inability to visualize the nuclear pre-replication complex in wild-type GSCs. Together, this leads to the model that a pool of CDK-2 is inactive, which enables loading of the pre-replication complex, but that high CDK-2/CYE-1 levels throughout GSCs result in the loading being transient, thus facilitating an accelerated entry into S phase, effectively coupling the high expression of CDK-2 with the G1/S switch and abbreviation of G1.

Development (2018) 145, dev161042. doi:10.1242/dev.161042

DPL-1 as a transcriptional repressor of CDK-2 to regulate G1- and S-phase progression

DP1/E2F proteins are canonical G1/S-phase regulators across multiple systems, where they promote G1/S-phase progression through activation of S-phase target genes. However, in *C. elegans* loss of *dpl-1* had not previously revealed any loss of G1/S phase in the proliferative cells either in the soma (Ceol and Horvitz, 2001; Chi and Reinke, 2006; Reddien et al., 2007) or the germline (this study). These data suggested that DP1/E2F may not function canonically to promote proliferative S phase in *C. elegans*. Instead, in this study, we discovered that genetically DPL-1 repressed *cdk-2* mRNA accumulation, and together with the modEncode data, we infer that DPL-1 by binding to the CDK-2 intron 1 represses CDK-2 mRNA transcription and thus S-phase progression. Together with our observation that DPL-1 functions downstream to GSK-3 to control CDK-2 mRNA, we propose that under normal conditions, DPL-1 is inactivated by continuous expression of GSK-3, resulting in continuous high levels of CDK-2. EFL-1, the partner of DPL-1, is closest in homology to E2F4 family of E2F transcription factors (Smith et al., 1996), and in vertebrates E2F4 family members have been implicated in repression of S-phase target genes rather than activation (Dominguez-Brauer et al., 2009; Pilkinton et al., 2007; Popov et al., 2005). Thus, it is possible, that in *C. elegans*, the DPL-1/EFL-1 complex function more like the DP1/E2F4 complex in vertebrates and represses G1/S transition. Together, these data reveal a novel mode of cell cycle regulation via transcriptional control of cyclin dependent kinases.

MATERIALS AND METHODS

C. elegans strains and culture

Standard culture conditions were used with maintenance at 20°C unless otherwise noted (Brenner, 1974). Temperature-sensitive strains containing *glp-1(bn18ts)* or *glp-1(ar202gf)* were maintained at 15°C and were shifted to 25°C as embryos along with controls for experiments. Details on the construction of GFP::GSK-3 transgenes, the CDK-2 promoter and intron transcriptional reporter transgenes, the generation of the transgenic lines, and the characterization of *gsk-3* mutant alleles are available in the supplementary Materials and Methods and Table S2.

Larval germ cell counts

Germ cell counts were performed using whole-mount visualization of *zuIs252*[PGL-1::mRFP] and DAPI. Counts were performed at L1, early L2, early L3 and early L4 in both wild-type and two *gsk-3* alleles (*tm2223* and *nr2047*).

EdU labeling

EdU feeding experiments were performed as described previously (Fox et al., 2011). Soaking EdU experiments were performed with worms grown on nematode growth medium (NGM) plates with *E. coli* OP50 bacteria as required, washed three times with M9T (M9 buffer, 0.1% Tween 20) and transferred to a flat-bottomed 48-well plate, followed by incubation with 200 µM EdU solution for 10 min at room temperature in the dark. The animals were then dissected and germlines processed using the Click-iT Plus EdU Alexa Fluor 594 Imaging Kit (ThermoFisher Scientific, catalog number C10639) per the manufacturer's recommendations, with a minor modification. Instead of the copper protectant provided with the kit (Component E), 2 mM $CuSO_4$ (final concentration) was used.

Antibodies

The following antibodies were used: anti-HIM-3 (Sdix), anti-REC-8 (Novus), anti-phospho-Histone H3 (Ser10) (Millipore), anti-GFP (Novus Biologicals), anti-CYE-1 [Dr Edward T. Kipreos (University of Georgia, Athens, GA, USA)], Gp-anti-lamin [Dr Kelly Liu (Cornell University, Ithaca, NY, USA)], anti-β-tubulin (Sigma), and donkey anti-mouse Alexa 594, goat anti-mouse Alexa Cy5, goat anti-mouse Alexa 488, goat anti-rabbit Alexa 488, goat anti-guinea pig Alexa 594, anti-rabbit HRP and anti-mouse HRP secondary antibodies (Molecular Probes).

Germline dissection and staining

All animals were dissected as adults 24 h after the L4 stage of development, unless otherwise mentioned. Germlines were dissected and stained as described previously (Arur et al., 2011, 2009; Drake et al., 2014; Suen et al., 2013).

PLP mounting for GFP visualization

To assay the transcriptional reporter GFP worms, *vizSi32*[*Intron cdk-2::NLS::GFP::tbb-2 3′UTR*], *wt* and *gsk-3(nr2047)* were dissected in the same dish 24 h after L4 in PBST and fixed for 3 min using 4% PLP (periodate/lysine/paraformaldehyde) (Hixson et al., 1981) with 4 µg/ml DAPI. After washing the fixed germlines three times, germlines were mounted on a 2% agarose pad and observed immediately. The pictures were taken on the same slide with identical exposure and gain for the GFP channel.

Image acquisition and processing on Zeiss Axio imager

Each image was captured with overlapping cell (Arur et al., 2009) boundaries using 40× or 63× objectives to make the montage. The focal plane was maintained throughout the experiment. All images were taken on a Zeiss Axio Imager upright microscope by using AxioVs40 V4.8.2.0 SP1 micro-imaging software and a Zeiss Axio MRm camera. The montages were then assembled in Adobe Photoshop CS5.1 and processed identically.

Quantitative real-time PCR (qRT-PCR)

Total RNA was isolated from at least 100 dissected germlines using the miRNeasy Mini Kit (Qiagen). cDNA was synthesized from 500 ng of total RNA using the iScript cDNA Synthesis Kit (Bio-Rad Laboratories). cDNA was amplified for qRT-PCR using iTaq Universal SYBR Green Supermix (Bio-Rad Laboratories) according to the manufacturer's instructions. Amplified cDNA was monitored after each cycle and measured ΔCt in the CFX96 Real time system (Bio-Rad Laboratories). The relative expression rate was determined using the ΔCt method as described in the manufacturer's instructions (Bio-Rad Laboratories). Average expression of the reference gene *act-1* was used to control for template levels. For further details of primers, see the supplementary Materials and Methods.

RNA interference (RNAi) analysis

RNAi was performed by feeding as described previously (Arur et al., 2009). *cdk-2*, *cye-1*, *dpl-1*, *efl-1* and *lin-35* RNAi clones (Vidal ORFeome Library, or Ahringer RNAi library) were sequence verified and grown overnight on solid LB agar plates containing 100 µg/ml of ampicillin and 50 µg/ml of tetracycline at 37°C. Single colonies were then inoculated in LB liquid cultures containing 100 µg/ml of ampicillin and 50 µg/ml of tetracycline, and grown to the necessary densities as described previously (Arur et al., 2009). The cultures were then seeded onto the standard NGM agar plates supplemented with 1 mM isopropyl β-D-1-thiogalactopyranoside (IPTG) and containing 100 µg/ml of ampicillin and 50 µg/ml of tetracycline. For P0 RNAi, L4 stage wild-type or *gsk-3* homozygous mutants were transferred to RNAi plates and dissected for analysis after 48 h. For F1 RNAi, L4 stages of wild-type or *gsk-3* heterozygous animals were allowed to lay progeny on the RNAi plates for 24 h, and transferred to a fresh RNAi plate every 24 h for an additional 3 days. Wild-type and *gsk-3* homozygous F1 progeny from these plates were then synchronized at mid-L4 stage and dissected for analysis at 48 h past mid-L4.

Western blot analysis

Wild-type (N2), and GFP::GSK-3 L4 hermaphrodites were hand-picked (250 for each lane), grown for 24 h and then harvested for western blot analysis as previously described (Arur et al., 2009, 2011). The extracts were resolved on 10% SDS-PAGE, transferred to PVDF membrane, and probed with antibodies to GFP (Novus Biologicals) and β-tubulin (1:1000). Western blots were developed using SuperSignal West Pico Chemiluminescent Substrate (Pierce) on Kodak BioMax MS films.

Hairpin chain reaction-based *in situ* mRNA hybridization

cdk-2 mRNA FISH was performed using hairpin chain reaction as described previously (Huang et al., 2016; Wei et al., 2016; Xuan and Hsing, 2014), except that the analysis in the present study was conducted on dissected germlines that were fixed in a 3% paraformaldehyde and 0.25% glutaraldehyde solution at room temperature for 2 h. The probes were obtained from Molecular Instruments and the manufacturer's instructions were followed.

Confocal analysis of nuclei sizes

Wild-type and *gsk-3(nr2047)* germlines were dissected and stained with DAPI and Gp-anti-lamin (1:200). Germlines were mounted in Vectashield and allowed to settle overnight at 4°C in dark. *Z*-stack images of the entire mitotic zone were acquired using a Nikon A1 laser scanning confocal microscope with a 60× oil objective (*z* step=0.5 µm). Images were deconvolved using AutoQuant X3 (20 iteration) and cell sizes were analyzed using ImageJ. The middle planes of the nuclei were selected and nuclei sizes were quantified by measuring the circumference of each nucleus based on lamin staining. A total of 471 (from five animals) and 404 nuclei (from seven animals) were analyzed for wild type and *gsk-3(nr2047)*, respectively.

Measuring progenitor zone length, M-phase and S-phase indices

Progenitor zone length was measured spatially as the distance from the distal tip to the first HIM-3-positive nucleus that developed. Each nucleus was visualized by DAPI. The M-phase index was calculated as the number of pH3-positive cells in the progenitor zone over the total number of cells in the progenitor zone ×100. S-phase index was calculated as the number of EdU-positive cells in the progenitor zone out of the total number of cells in the progenitor zone ×100. The criterion used for distinguishing the progenitors from meiotic cells was the HIM-3 boundary.

Acknowledgements

We thank Dr Jane Hubbard and members of the Arur Lab for critical comments on the manuscript and helpful discussions. We thank Jessica Chen for technical help with Fig. S5A. Worm strains were obtained from *C. elegans* Genetics stock center at University of Minnesota funded by the National Institutes of Health (P40 OD010440) and from Dr Shohei Mitani (NBRP, Japan). We thank Dr Hyman for the CDK-2 transgenic line *ddIs30*.

Competing interests

The authors declare no competing or financial interests.

Author contributions

Conceptualization: T.F., H.-J.J., S.A.; Methodology: T.F., H.-J.J., K.A.T.; Validation: H.-J.J., K.A.T., S.-Y.C.; Formal analysis: T.F., S.A.; Investigation: T.F., H.-J.J., K.A.T., S.-Y.C., S.A.; Writing - original draft: T.F., K.A.T., S.A.; Writing - review & editing: T.F., K.A.T., S.A.; Supervision: S.A.; Project administration: S.A.; Funding acquisition: S.A.

Funding

This work is funded by the National Institutes of Health (GM98200 to S.A. and GM98200S1 to K.A.T.), by the American Cancer Society (RSG014044DDC to S.A.), by the Cancer Prevention and Research Institute of Texas (RP160023 to S.A.) and by Anna Fuller Funds (to S.A.). S.A. is an Andrew Sabin Family Foundation Fellow at the University of Texas MD Anderson Cancer Center. Deposited in PMC for release after 12 months.

Supplementary information

Supplementary information available online at
http://dev.biologists.org/lookup/doi/10.1242/dev.161042.supplemental

References

Aleem, E., Kiyokawa, H. and Kaldis, P. (2005). Cdc2-cyclin E complexes regulate the G1/S phase transition. *Nat. Cell Biol.* **7**, 831-836.

Almasan, A., Yin, Y., Kelly, R. E., Lee, E. Y., Bradley, A., Li, W., Bertino, J. R. and Wahl, G. M. (1995). Deficiency of retinoblastoma protein leads to inappropriate S-phase entry, activation of E2F-responsive genes, and apoptosis. *Proc. Natl. Acad. Sci. USA* **92**, 5436-5440.

Arur, S., Ohmachi, M., Nayak, S., Hayes, M., Miranda, A., Hay, A., Golden, A. and Schedl, T. (2009). Multiple ERK substrates execute single biological processes in Caenorhabditis elegans germ-line development. *Proc. Natl. Acad. Sci. USA* **106**, 4776-4781.

Arur, S., Ohmachi, M., Berkseth, M., Nayak, S., Hansen, D., Zarkower, D. and Schedl, T. (2011). MPK-1 ERK controls membrane organization in C. elegans oogenesis via a sex-determination module. *Dev. Cell* **20**, 677-688.

Austin, J. and Kimble, J. (1987). glp-1 is required in the germ line for regulation of the decision between mitosis and meiosis in C. elegans. *Cell* **51**, 589-599.

Berry, L. W., Westlund, B. and Schedl, T. (1997). Germ-line tumor formation caused by activation of glp-1, a Caenorhabditis elegans member of the Notch family of receptors. *Development* **124**, 925-936.

Blow, J. J. (1993). Preventing re-replication of DNA in a single cell cycle: evidence for a replication licensing factor. *J. Cell Biol.* **122**, 993-1002.

Blow, J. J. and Hodgson, B. (2002). Replication licensing–defining the proliferative state? *Trends Cell Biol.* **12**, 72-78.

Bouskila, M., Hirshman, M. F., Jensen, J., Goodyear, L. J. and Sakamoto, K. (2008). Insulin promotes glycogen synthesis in the absence of GSK3 phosphorylation in skeletal muscle. *Am. J. Physiol. Endocrinol. Metab.* **294**, E28-E35.

Brenner, S. (1974). The genetics of Caenorhabditis elegans. *Genetics* **77**, 71-94.

Campbell, J. M., Nottle, M. B., Vassiliev, I., Mitchell, M. and Lane, M. (2012). Insulin increases epiblast cell number of in vitro cultured mouse embryos via the PI3K/GSK3/p53 pathway. *Stem Cells Dev.* **21**, 2430-2441.

Ceol, C. J. and Horvitz, H. R. (2001). dpl-1 DP and efl-1 E2F act with lin-35 Rb to antagonize Ras signaling in C. elegans vulval development. *Mol. Cell* **7**, 461-473.

Chi, W. and Reinke, V. (2006). Promotion of oogenesis and embryogenesis in the C. elegans gonad by EFL-1/DPL-1 (E2F) does not require LIN-35 (pRB). *Development* **133**, 3147-3157.

Chi, W. and Reinke, V. (2009). DPL-1 (DP) acts in the germ line to coordinate ovulation and fertilization in C. elegans. *Mech. Dev.* **126**, 406-416.

Chong, J. P. J. and Blow, J. J. (1996). DNA replication licensing factor. *Prog. Cell Cycle Res.* **2**, 83-90.

Chuykin, I. A., Lianguzova, M. S., Pospelova, T. V. and Pospelov, V. A. (2008). Activation of DNA damage response signaling in mouse embryonic stem cells. *Cell Cycle* **7**, 2922-2928.

Cotsarelis, G., Sun, T.-T. and Lavker, R. M. (1990). Label-retaining cells reside in the bulge area of pilosebaceous unit: implications for follicular stem cells, hair cycle, and skin carcinogenesis. *Cell* **61**, 1329-1337.

Cowan, C. R. and Hyman, A. A. (2006). Cyclin E-Cdk2 temporally regulates centrosome assembly and establishment of polarity in Caenorhabditis elegans embryos. *Nat. Cell Biol.* **8**, 1441-1447.

Crittenden, S. L., Eckmann, C. R., Wang, L., Bernstein, D. S., Wickens, M. and Kimble, J. (2003). Regulation of the mitosis/meiosis decision in the Caenorhabditis elegans germline. *Philos. Trans. R. Soc. Lond. B Biol. Sci.* **358**, 1359-1362.

Doble, B. W. and Woodgett, J. R. (2003). GSK-3: tricks of the trade for a multi-tasking kinase. *J. Cell Sci.* **116**, 1175-1186.

Dominguez-Brauer, C., Chen, Y.-J., Brauer, P. M., Pimkina, J. and Raychaudhuri, P. (2009). ARF stimulates XPC to trigger nucleotide excision repair by regulating the repressor complex of E2F4. *EMBO Rep.* **10**, 1036-1042.

Drake, M., Furuta, T., Suen, K. M., Gonzalez, G., Liu, B., Kalia, A., Ladbury, J. E., Fire, A. Z., Skeath, J. B. and Arur, S. (2014). A requirement for ERK-dependent Dicer phosphorylation in coordinating oocyte-to-embryo transition in C. elegans. *Dev. Cell* **31**, 614-628.

Edgar, L. G. and McGhee, J. D. (1988). DNA synthesis and the control of embryonic gene expression in C. elegans. *Cell* **53**, 589-599.

Elsner, M. and Mak, H. C. (2011). A modENCODE snapshot. *Nat. Biotechnol.* **29**, 238-240.

Fox, P. M. and Schedl, T. (2015). Analysis of germline stem cell differentiation following loss of GLP-1 notch activity in caenorhabditis elegans. *Genetics* **201**, 167-184.

Fox, P. M., Vought, V. E., Hanazawa, M., Lee, M. H., Maine, E. M. and Schedl, T. (2011). Cyclin E and CDK-2 regulate proliferative cell fate and cell cycle progression in the C. elegans germline. *Development* **138**, 2223-2234.

Garcia-Muse, T. and Boulton, S. J. (2005). Distinct modes of ATR activation after replication stress and DNA double-strand breaks in Caenorhabditis elegans. *EMBO J.* **24**, 4345-4355.

Gleason, J. E., Szyleyko, E. A. and Eisenmann, D. M. (2006). Multiple redundant Wnt signaling components function in two processes during C. elegans vulval development. *Dev. Biol.* **298**, 442-457.

Graham, C. F. (1966a). The effect of cell size and DNA content on the cellular regulation of DNA synthesis in haploid and diploid embryos. *Exp. Cell Res.* **43**, 13-19.

Graham, C. F. (1966b). The regulation of DNA synthesis and mitosis in multinucleate frog eggs. *J. Cell Sci.* **1**, 363-374.

Guevara, C., Korver, W., Mahony, D., Parry, D., Seghezzi, W., Shanahan, F. and Lees, E. (1999). Regulation of G1/S transition in mammalian cells. *Kidney Int.* **56**, 1181-1192.

Hansen, D. and Schedl, T. (2013). Stem cell proliferation versus meiotic fate decision in Caenorhabditis elegans. *Adv. Exp. Med. Biol.* **757**, 71-99.

Hansen, D., Hubbard, E. J. and Schedl, T. (2004). Multi-pathway control of the proliferation versus meiotic development decision in the Caenorhabditis elegans germline. *Dev. Biol.* **268**, 342-357.

Hixson, D. C., Yep, J. M., Glenney, J. R., Jr, Hayes, T. and Walborg, E. F. Jr (1981). Evaluation of periodate/lysine/paraformaldehyde fixation as a method for cross-linking plasma membrane glycoproteins. *J. Histochem. Cytochem.* **29**, 561-566.

Huang, J., Khan, I., Liu, R., Yang, Y. and Zhu, N. (2016). Single primer-mediated circular polymerase chain reaction for hairpin DNA cloning and plasmid editing. *Anal. Biochem.* **500**, 18-20.

Jaramillo-Lambert, A., Ellefson, M., Villeneuve, A. M. and Engebrecht, J. (2007). Differential timing of S phases, X chromosome replication, and meiotic prophase in the C. elegans germ line. *Dev. Biol.* **308**, 206-221.

Kermi, C., Lo Furno, E. and Maiorano, D. (2017). Regulation of DNA replication in early embryonic cleavages. *Genes (Basel)* **8**, E42.

Kimble, J. and Crittenden, S. L. (2005). *Germline Proliferation and its Control*. In WormBook (ed. The C. elegans Research Community) .

Larner, J., Villar-Palasi, C., Goldberg, N. D., Bishop, J. S., Huijing, F., Wenger, J.-I., Sasko, H. and Brown, N. B. (1968). Hormonal and non-hormonal control of glycogen synthesis-control of transferase phosphatase and transferase I kinase. *Adv. Enzyme Regul.* **6**, 409-423.

Li, J., Deng, M., Wei, Q., Liu, T., Tong, X. and Ye, X. (2011). Phosphorylation of MCM3 protein by cyclin E/cyclin-dependent kinase 2 (Cdk2) regulates its function in cell cycle. *J. Biol. Chem.* **286**, 39776-39785.

Maduro, M. F., Meneghini, M. D., Bowerman, B., Broitman-Maduro, G. and Rothman, J. H. (2001). Restriction of mesendoderm to a single blastomere by the combined action of SKN-1 and a GSK-3beta homolog is mediated by MED-1 and -2 in C. *elegans*. *Mol Cell* **7**, 475-485.

McManus, E. J., Sakamoto, K., Armit, L. J., Ronaldson, L., Shpiro, N., Marquez, R. and Alessi, D. R. (2005). Role that phosphorylation of GSK3 plays in insulin and Wnt signalling defined by knockin analysis. *EMBO J.* **24**, 1571-1583.

Morrison, S. J. and Spradling, A. C. (2008). Stem cells and niches: mechanisms that promote stem cell maintenance throughout life. *Cell* **132**, 598-611.

Muers, M. (2011). Functional genomics: the modENCODE guide to the genome. *Nat. Rev. Genet.* **12**, 80.

Müller, H., Moroni, M. C., Vigo, E., Petersen, B. O., Bartek, J. and Helin, K. (1997). Induction of S-phase entry by E2F transcription factors depends on their nuclear localization. *Mol. Cell. Biol.* **17**, 5508-5520.

Ohtsuka, S. and Dalton, S. (2008). Molecular and biological properties of pluripotent embryonic stem cells. *Gene Ther.* **15**, 74-81.

Parisi, F., Riccardo, S., Daniel, M., Saqcena, M., Kundu, N., Pession, A., Grifoni, D., Stocker, H., Tabak, E. and Bellosta, P. (2011). Drosophila insulin and target of rapamycin (TOR) pathways regulate GSK3 beta activity to control Myc stability and determine Myc expression in vivo. *BMC Biol.* **9**, 65.

Pilkinton, M., Sandoval, R. and Colamonici, O. R. (2007). Mammalian Mip/LIN-9 interacts with either the p107, p130/E2F4 repressor complex or B-Myb in a cell cycle-phase-dependent context distinct from the Drosophila dREAM complex. *Oncogene* **26**, 7535-7543.

Popov, B., Chang, L.-S. and Serikov, V. (2005). Cell cycle-related transformation of the E2F4-p130 repressor complex. *Biochem. Biophys. Res. Commun.* **336**, 762-769.

Reddien, P. W., Andersen, E. C., Huang, M. C. and Horvitz, H. R. (2007). DPL-1 DP, LIN-35 Rb and EFL-1 E2F act with the MCD-1 zinc-finger protein to promote programmed cell death in Caenorhabditis elegans. *Genetics* **175**, 1719-1733.

Rylatt, D. B., Aitken, A., Bilham, T., Condon, G. D., Embi, N. and Cohen, P. (1980). Glycogen synthase from rabbit skeletal muscle. Amino acid sequence at the sites phosphorylated by glycogen synthase kinase-3, and extension of the N-terminal sequence containing the site phosphorylated by phosphorylase kinase. *Eur. J. Biochem.* **107**, 529-537.

Schultz, E. (1974). A quantitative study of the satellite cell population in postnatal mouse lumbrical muscle. *Anat. Rec.* **180**, 589-595.

Schultz, E. (1985). Satellite cells in normal, regenerating and dystrophic muscle. *Adv. Exp. Med. Biol.* **182**, 73-84.

Seidel, H. S. and Kimble, J. (2015). Cell-cycle quiescence maintains Caenorhabditis elegans germline stem cells independent of GLP-1/Notch. *Elife* **4**, e10832.

Shah, S., Lubeck, E., Schwarzkopf, M., He, T. F., Greenbaum, A., Sohn, C. H., Lignell, A., Choi, H. M., Gradinaru, V., Pierce, N. A. et al. (2016). Single-molecule RNA detection at depth by hybridization chain reaction and tissue hydrogel embedding and clearing. *Development* **143**, 2862-2867.

Shirayama, M., Soto, M. C., Ishidate, T., Kim, S., Nakamura, K., Bei, Y., van den Heuvel, S. and Mello, C. C. (2006). The Conserved Kinases CDK-1, GSK-3, KIN-19, and MBK-2 Promote OMA-1 Destruction to Regulate the Oocyte-to-Embryo Transition in C. *elegans*. *Curr. Biol.* **16**, 47-55.

Smith, E. J., Leone, G., DeGregori, J., Jakoi, L. and Nevins, J. R. (1996). The accumulation of an E2F-p130 transcriptional repressor distinguishes a G0 cell state from a G1 cell state. *Mol. Cell. Biol.* **16**, 6965-6976.

Snow, M. H. (1977). The effects of aging on satellite cells in skeletal muscles of mice and rats. *Cell Tissue Res.* **185**, 399-408.

Sonneville, R., Querenet, M., Craig, A., Gartner, A. and Blow, J. J. (2012). The dynamics of replication licensing in live Caenorhabditis elegans embryos. *J. Cell Biol.* **196**, 233-246.

Stead, E., White, J., Faast, R., Conn, S., Goldstone, S., Rathjen, J., Dhingra, U., Rathjen, P., Walker, D. and Dalton, S. (2002). Pluripotent cell division cycles are driven by ectopic Cdk2, cyclin A/E and E2F activities. *Oncogene* **21**, 8320-8333.

Suen, K. M., Lin, C.-C., George, R., Melo, F. A., Biggs, E. R., Ahmed, Z., Drake, M. N., Arur, S., Arold, S. T. and Ladbury, J. E. (2013). Interaction with Shc prevents aberrant Erk activation in the absence of extracellular stimuli. *Nat. Struct. Mol. Biol.* **20**, 620-627.

Sutherland, C., Leighton, I. A. and Cohen, P. (1993). Inactivation of glycogen synthase kinase-3 beta by phosphorylation: new kinase connections in insulin and growth-factor signalling. *Biochem. J.* **296**, 15-19.

Takada, S. and Cha, B. J. (2011). In vivo live-analysis of cell cycle checkpoints in Drosophila early embryos. *Methods Mol. Biol.* **782**, 75-92.

Wei, Y., Zhou, W., Li, X., Chai, Y., Yuan, R. and Xiang, Y. (2016). Coupling hybridization chain reaction with catalytic hairpin assembly enables non-enzymatic and sensitive fluorescent detection of microRNA cancer biomarkers. *Biosens. Bioelectron.* **77**, 416-420.

White, J. and Dalton, S. (2005). Cell cycle control of embryonic stem cells. *Stem Cell Rev.* **1**, 131-138.

Xuan, F. and Hsing, I.-M. (2014). Triggering hairpin-free chain-branching growth of fluorescent DNA dendrimers for nonlinear hybridization chain reaction. *J. Am. Chem. Soc.* **136**, 9810-9813.

Ying, Q.-L., Wray, J., Nichols, J., Batlle-Morera, L., Doble, B., Woodgett, J., Cohen, P. and Smith, A. (2008). The ground state of embryonic stem cell self-renewal. *Nature* **453**, 519-523.

Zetka, M. C., Kawasaki, I., Strome, S. and Muller, F. (1999). Synapsis and chiasma formation in Caenorhabditis elegans require HIM-3, a meiotic chromosome core component that functions in chromosome segregation. *Genes Dev.* **13**, 2258-2270.